Nonlinear Analysis: Modelling and Control, Vol. 29, No. 3, 562–587
https://doi.org/10.15388/namc.2024.29.35107

Vilnius University Press

Delay-induced nutrient recycling in plankton system: Application to Sundarban mangrove wetland

Ravikant Singh[a], **Archana Ojha**[a], **Nilesh Kumar Thakur**[a], **Ranjit Kumar Upadhyay**[b]

[a]Department of Mathematics, National Institute of Technology, Raipur (CG) - 492010, India
singhravikant2695@gmail.com; archanaojha1991@gamil.com; nkthakur.maths@nitrr.ac.in

[b]Department of Mathematics and Computing, Indian Institute of Technology (Indian School of Mines), Dhanbad, Jharkhand 826004, India
ranjit.chaos@gmail.com

Received: March 25, 2023 / **Revised:** January 3, 2023 / **Published online:** April 17, 2024

Abstract. The paper discusses the nutrient–plankton system with effect of time delay in nutrient recycling and toxin-determined function response (TDFR). The designed model system explores the delay-induced system dynamics. We present the local stability analysis of interior equilibrium points in absence as well as in presence of time delay. Further, the direction of Hopf bifurcation is obtained. We perform the numerical computation and observe that time delay in nutrient recycling can generate the periodic solution in a stable nutrient–plankton system. Some other essential parameters, such as input concentration of nutrients and natural removal rate of nutrients, also regulate the dynamical system. The system shows Hopf and double-Hopf bifurcation in the presence of time delay. Our study shows that the delay in the nutrient recycling causes instability transition phenomenon. The delay-induced nutrient recycling and different input concentrations of nutrients can regulate the estuarine system. Finally, the stability switching is observed for delayed system.

Keywords: nutrient cycling, TDFR, stability, bifurcation, time delay.

1 Introduction

Wetland ecosystems, the area flooded by water, either seasonally or permanently, help the livelihoods of millions of people living in them or surrounding them. It provides a rich natural biodiverse habitat including food, soil, water, and various ranges of the plankton community, fish, and birds and encourages a high diversity of flora and fauna. Wetlands enhance the water quality and make the ecosystem productive and rich with nutrients for better survival in the natural environment. Sundarban wetland ecosystem is the most extensive contiguous mangrove forest situated in the southwest of Bangladesh and adjoint to the Bay of Bengal. The mangrove area of Sundarban constituted the deltaic

estuarine of three major rivers Ganges, Brahmaputra, and Meghna. It formed the world's most dynamic estuarine with significant economic value. The Sundarban [$88°05'$ to $89°51'$E and $21°32'$ to $22°-40'$N] shared approximate 10000 km^2 area between two countries, India and Bangladesh, in which around 38% area of the total mangrove shared by India, and the rest part (i.e., 62%) shared by Bangladesh. The varying freshwater inputs of Sundarban contain 24 mangrove taxa with 9 distinct families. The biodiversity of Sundarbans embraces around 350 plants, 300 birds, 250 fishes. Besides them, numerous community of phytoplankton, zooplankton, bacteria, fungi, reptiles, mammals, benthic invertebrates, etc. [12]. The Sundarbans estuary has recorded with 46 taxa of phytoplankton belonging to six algal groups of diatoms (*Bacillariophyceae*), is followed by green algae (*Chlorophyceae*) and blue-green algae (*Cyanophyceae*) [19]. Sundarbans mangrove has been suffering from severe threats from excessive growth of toxic algal bloom [31]. Several species are perceived in Sundarban, which is now dominated by harmful algal blooms (HABs) and become a major issue in front of biological researchers. An increase in input concentration of nutrients may cause the toxic algal bloom that has a negative impact on zooplankton and finally on fish production. Many scientific studies indicate that the water quality of the Sundarbans estuary degraded by toxic *Dinoflagellates* and *Cyanographyceaes*. This type of event puts the question mark on the survival of mangroves. To conserve the Sundarbans ecosystem from the adverse effects of the toxin, monitoring the occurrence of such blooms is essential from a biological perspective. Recently, Thakur et al. [30] analyzed the adverse consequence of toxic phytoplankton in a diffusion induced plankton model for the Sundarban wetland with time delay.

Mathematical modeling of wetland and aquatic ecosystem provides a key tool to study the dynamical properties of different levels of interaction among marine species. Many authors have studied that nutrient availability (nitrogen, phosphorous, sulphur, etc.) highly affects the growth of the plankton community by limiting their maturation and procreation process [15]. Utilization of any resource is the critical element of interactions of marine microbial ecosystems. A high concentration of nutrients with a favourable environment supports the massive growth of blooms (i.e., microbial species). Generally, nutrients may generate automatically from the various natural sources of concentrations in the estuarine and aquatic environments. Although, estuary also plays a major role in the reproduction of nutrients from high mangrove vegetations of litterfall, decomposition of leaves as well as dead phytoplankton, and other litters through transportation in the estuarine water [8]. Fan et al. [10] have investigated the various characteristics of nutrients concentration in a water ecosystem. Zhang and Wang [35] carried a detailed study about the bistable phenomenon on the nutrient–phytoplankton–zooplankton population model by choosing the input rate of nutrient as a bifurcation parameter. Bairagi et al. [1] developed a four-component population model (involving nutrient, nontoxic phytoplankton (NTP), toxin-producing phytoplankton (TPP), and zooplankton). They studied the environmental factors that are significantly responsible for complexity. Any dynamical system becomes more complex when the species adopted some strategy to maintain their survivorship. Toxicity is one of them that acts universally in the aquatic system to sustain the high diversity of the planktonic community and opposing the grazing pressure [27]. Some studies revealed that toxicity has strong influence on the dynamical structure of

a nutrient–plankton system [24]. Chakraborty et al. [3] analyzed the nutrient–TPP model under the consideration of nutrient recycling. They attempted to understand the nutrient recycling phenomena in recurring blooms. Chakraborty et al. [4] deliberated the spatial complexity with the effect of toxin substance and observed the different spatial oscillation for a diffusive nutrient plankton system.

One of the most commonly employed descriptions of the phytoplankton consumption by the zooplankton is the traditional Holling type II functional response [14], which assumes that the growth rate of zooplankton is a monotonically increasing function of phytoplankton density. However, this will not be appropriate if the chemical defense of phytoplanktons is considered, in which case the negative effect of phytoplankton toxin on zooplankton can lead to a decrease in the growth rate when the plant density is high. To explore the impact of plant toxicity on the dynamics of plankton interactions, TDFR developed [11]. The toxin-determined functional response is a modification of the traditional Holling type II response by including the negative effect of toxin on zooplankton growth, which can overwhelm the positive effect of biomass ingestion at sufficiently high phytoplankton toxicant concentrations [2]. Liu et al. [18] discussed a plant–herbivore model with TDFR and demonstrated the bifurcation analysis in detail. Chatterjee and Pal [5] have studied a nutrient–plankton system with TDFR. They observed that in order to maintain the stable nature of the system, certain parameters have to control. Recently, Ji and Wang [16] established some exciting results regarding the control and occurrence of phytoplankton blooms through stability and bifurcation examination for a nutrient–phytoplankton system with toxic effect. Upadhyay et al. [32] considered a TDFR reaction–diffusion system for nutrient–plankton density and established the spatial distribution of the biotic subsystem.

Another crucial component that has an important impact on the diverse population of a biological system is the involvement of time delay that can produce more rational outcomes and make fluctuation in the entire dynamical systems [23]. Biologically, every species requires digestion time delay after consuming their meal prior to further activities [17]. Nutrient availability in the estuarine system is also influenced by the consideration of time delay as litterfall and their transportation in estuary needed some time lag [20]. Das and Ray [9] briefly elaborated on the stability features of the delayed plankton system with nutrient recycling and observed that nutrient recycling does not change the stability criteria. There are numerous studies on plankton dynamics where the importance of delay has been well explored [22]. Xiao and Chen [34] suggested that incorporation of discrete-time delay in a complex prey–predator system have enough potential to stabilize as well as destabilize the dynamics. Thakur et al. [28] analyzed the simultaneous effect of multiple delays for a plankton–fish system and shown the existence of transcritical bifurcation for the system. They have also found the chaotic attractor for the equal magnitude of delays. Cui and Yan [6] have discussed the dynamical feature of multiple delays for the tri-trophic food chain system based on the Lotka–Volterra scheme and obtained the phenomenon of stability loss and various oscillations. Many research articles have focused on the study of delay induced nutrient–plankton model system [7]. Thakur et al. [29] explored a nutrient–plankton system with delay to review the impact of phytoplankton toxicity, which causes the extra morality of zooplankton in the system dynamics and found

chaotic oscillations through stability switching for the high value of toxin maturation delay. Singh et al. [25] studied a diffusive nutrient–plankton system and observed that the liberation of toxins stabilizes/destabilizes the system in the presence of time delay. Wang et al. [33] analyzed the dynamics of nutrient cycling with time delay in the nutrient–plankton model and obtained stability switching phenomenon due to time lag. Most of the studies based on either wastewater treatment or the investigation of the spatial structure of the wetland ecosystem, but very few focused on studying time delay in a wetland ecosystem. The inclusion of time delay makes the system's biological relevance and helps to more precisely analyze the interacting organisms and thus provide an effective understanding of the ecosystem's application [21].

With the view of above, we have studied a simple nutrient–phytoplankton–zooplankton population model with nutrient recycling and the consequence of toxicity in plankton's dynamics under the consideration of TDFR [5, 18, 32, 33]. The nutrient uptake and phytoplankton toxicity functions are taken as Holling type II response function and TFDR. Under the consideration of the work done by [33], a discrete-time delay introduced in nutrient recycling terms in the nutrient dynamics. The main objective of the present work is to examine the role of some crucial parameters that affect the wetland environment widely. Investigation of time delay with different nutrient levels provides more general findings to understand the nutrient–plankton dynamics.

2 Formulation of nutrient–plankton model system

In an aquatic ecosystem, some plankton species are influenced by chemical defenses that explicitly reduce the consumption rate of zooplankton. Recently, Upadhyay et al. [32] analyzed the significance of TDFR on the nutrient–plankton dynamics to guide exploration and harvesting of microalgae. We have proposed a nutrient–plankton interaction model, which is made up of nutrient that interact with the plankton community in an estuarine system. At any instant of time t, nutrient, phytoplankton, and zooplankton are represented as $N(t)$, $P(t)$, and $Z(t)$, respectively. The change in nutrients concentration and species biomass is described as

$$\begin{aligned}
\dot{N} &= \text{input} - \text{loss} - \text{uptake} + \text{recycling},\\
\dot{P} &= \text{uptake} - \text{grazing by } Z - \text{death},\\
\dot{Z} &= \text{growth} - \text{death}.
\end{aligned}$$

The following assumptions are considered to formulate the model system:

(i) The dynamics is arising due to the coupling of nutrient $N(t)$, phytoplankton $P(t)$, and zooplankton $Z(t)$.

(ii) The model system receives a fixed outer source of input concentration of nutrient α, which is affected by the deterioration process of dead phytoplankton. Due to sedimentation, the term δN defines natural absorption rate of nutrients. Further, nutrient is recycled at the rate of κ after reaching senescence, which preserved the nutrient pool.

(iii) The nutrients are constantly available from wastewater discharges and sewage output in a quiet amount, even though phytoplankton cannot absorb an unlimited amount of nutrients. Thus, the nutrient uptake and conversion by phytoplankton are described by Holling type II, which is the most appropriate functional response biologically.

(iv) The phytoplankton toxicity on the feeding rates of zooplankton is considered as TDFR [5, 18]. The TDFR is discribed as

$$C(P) = \frac{wP}{1+hwP}\left(1 - \frac{wP}{4G_1(1+hwP)}\right),$$

where the term $wP/(4G_1(1+hwP))$ is in the Holling type II functional form. This functional form represents the detrimental impact of phytoplankton on zooplankton density.

(v) For phytoplankton, nutrients are the only preferred food source, whereas phytoplankton is the only preferred food source for zooplankton. Consequently, phytoplankton and zooplankton will die out at their natural death rates in the absence of preferred food.

With the above assumptions, mathematically the model system is described as

$$\begin{aligned}
\frac{\mathrm{d}N}{\mathrm{d}t} &= \alpha - \delta N - \frac{\beta NP}{a+N} + \kappa\gamma P,\\
\frac{\mathrm{d}P}{\mathrm{d}t} &= \frac{e\beta NP}{a+N} - C(P)Z - \gamma P,\\
\frac{\mathrm{d}Z}{\mathrm{d}t} &= mC(P)Z - \eta Z,
\end{aligned} \tag{1}$$

where

$$C(P) = \frac{wP}{1+hwP}\left(1 - \frac{wP}{4G_1(1+hwP)}\right), \quad w = e_1\sigma_1.$$

The schematic diagram for nutrient–plankton dynamical system is presented in Fig. 1. In model system (1), let α be the input concentration of nutrients flowing into the water, which is assumed to be constant, and δ is natural removal rate of nutrient in the form of sedimentation. The parameters β and $e\beta$ ($\beta \geqslant e\beta$) are the nutrient uptake rate for the

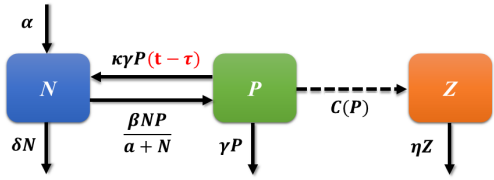

Figure 1. Schematic diagram for the model system (2).

Table 1. Definition of the parameters used in the model system (1) [5, 32].

Parameters	Description	Values	Units
α	Constant input concentration of nutrient	1	mg/m^{-3} day^{-1}
δ	Natural removal rate of nutrient	0.1	day^{-1}
β	Nutrient uptake rate for the phytoplankton	5	day^{-1}
e	Conversion rate of nutrient for the growth of phytoplankton population ($\beta \geqslant e\beta$)	0.933	–
a	Half saturation costant of phytoplankton	10	mg m^{-3}
e_1	Rate of encounter per unit of phytoplankton species	0.8	–
σ_1	Fraction of effort applied to foraging for plankton species	0.6	–
h	Handling time of the zooplankton	0.5	–
G_1	Max units of phytoplankton species a zooplankton can eat per day	3.5	–
γ, η	Mortality rates of plankton and zooplankton populations	0.7, 0.1	day^{-1}
m	Conversion efficiency of the zooplankton	0.5	–
κ	Nutrient recycling rate after the death of phytoplanktony	0.8	day^{-1}

phytoplankton population and conversion rate of nutrient for the growth of phytoplankton population, respectively. Since $C(P) = g(P)(1 - g(P)/(4G_1))$ is the TDFR, $g(P) = wP/(1 + hwP)$ is the cyrtoid-type functional response. The parameter w $(= e_1\sigma_1)$ is the product of resource encounter rate e_1 with food biomass fraction, which is ingested by the zooplankton, σ_1 $(0 < \sigma_1 \leqslant 1)$. The parameter e_1 depends on the radius of food item detection and movement velocity of zooplankton. The parameter h denotes the handling time per unit biomass. Let γ and η be the mortality rates of plankton and zooplankton populations. The parameter m is the conversion efficiency of the zooplankton. $\kappa\gamma$ is the nutrient recycling rate after the death of phytoplankton. The parameter $G_1 = M_1/T_1$, where M_1 is the maximum amount of toxin that a herbivore can consume per unit time, and T_1 is the amount of toxin per unit phytoplankton biomass.

The parameters and their usual meaning are given in Table 1, where all parameters are positive values.

To generalize the above discussed nutrient–plankton system, we have considered a biological situation in which the nutrient recycling from dead phytoplankton are assumed not to be an immediate process rather in the decomposition process of a few quantities κ $(0 < \kappa < 1)$ of dead phytoplankton into waste and ultimately transformed into nutrients after remineralization, some time delay is needed. Therefore, we have introduced a discrete-time delay τ in the nutrient recycling term of the equation. Hence, the corresponding delay-induced nutrient recycling model takes the following form:

$$\begin{aligned} \frac{\mathrm{d}N}{\mathrm{d}t} &= \alpha - \delta N - \frac{\beta NP}{a+N} + k\gamma P(t-\tau), \\ \frac{\mathrm{d}P}{\mathrm{d}t} &= \frac{e\beta NP}{a+N} - C(P)Z - \gamma P, \\ \frac{\mathrm{d}Z}{\mathrm{d}t} &= mC(P)Z - \eta Z \end{aligned} \tag{2}$$

with initial conditions

$$N(\theta) = \phi_1(\theta), \quad P(\theta) = \phi_2(\theta), \quad Z(\theta) = \phi_3(\theta) \quad \text{for all } \theta \in [-\tau, 0],$$

$$N(0) > 0, \qquad P(0) > 0, \qquad Z(0) > 0,$$

where $(\phi_1, \phi_2, \phi_3) \in C([-\tau, 0], \mathbb{R}^3_+)$, $\phi_1(0), \phi_2(0), \phi_3(0) > 0$.

3 Analysis and biological interpreation of delay-free model system

In this section, we analyze the model system (1). In this regard, first, we establish the boundedness of the system and then the stability of nonnegative biologically feasible equilibria.

Lemma 1. *Suppose* $\xi = \min\{\delta, (1-\kappa)\gamma, \eta\}$*, then all the solutions of the model system* (1)*, initiating in the interior of the positive octant*

$$\chi = \left\{ \big(N(t), P(t), Z(t)\big) \colon 0 \leqslant N(t) + \frac{1}{e}P(t) + \frac{1}{em}z(t) \leqslant \frac{\alpha}{\xi} \right\},$$

are positive and bounded for all $t \geqslant 0$.

The lemma shows that the model system (1) is nonnegative and bounded. It shows that the system is biologically well behaved.

The proof is deferred to Appendix A.

Under the equilibria analysis, the model system described by Eq. (1) possesses three nonnegative real equilibrium points: $E^0(\alpha/\delta, 0, 0)$, $E^1(\hat{N}, \hat{P}, 0)$, and $E^*(N^*, P^*, Z^*)$.

(i) The equilibrium point with nutrient only $E^0 = (\alpha/\delta, 0, 0)$ exists. Thus, the variational matrix $J(E^0)$ at E^0 is

$$J(E^0) = \begin{pmatrix} -\delta & -\frac{\beta\alpha}{(a\delta+\alpha)} + \kappa\gamma & 0 \\ 0 & \frac{e\beta\alpha}{(a\delta+\alpha)} - \gamma & 0 \\ 0 & 0 & -\eta \end{pmatrix}.$$

Eigenvalues around E^0 are $(-\delta, e\beta\alpha/(a\delta+\alpha)-\gamma, -\eta)$. The quantity $(e\beta\alpha/(a\delta+\alpha)-\gamma)$ is positive or negative according to $e\beta\alpha/(a\delta+\alpha) > \gamma$ or $e\beta\alpha/(a\delta+\alpha) < \gamma$. Thus, E^0 either locally asymptotically stable (LAS) or unstable depending on $e\beta\alpha/(a\delta+\alpha) - \gamma$.

(ii) The zooplankton-free equilibrium point $E^1 = (\hat{N}, \hat{P}, 0)$ exists on the NP-plane. We have

$$\alpha - \delta\hat{N} - \frac{\beta\hat{N}\hat{P}}{a+\hat{N}} + \kappa\gamma\hat{P} = 0, \qquad \frac{e\beta\hat{N}\hat{P}}{a+\hat{N}} - \gamma\hat{P} = 0.$$

Thus, we get

$$\hat{N} = \frac{a\gamma}{e\beta - \gamma}, \qquad \hat{P} = \frac{e(\alpha - \delta\hat{N})}{\gamma(1 - e\kappa)}.$$

The equilibrium point $E^1(\hat{N}, \hat{P}, 0)$ exists if the following conditions hold:

$$\text{(a) } e\beta > \gamma, \qquad \text{(b) } \alpha > \delta\hat{N}, \qquad \text{(c) } e\kappa < 1.$$

Thus, the variational matrix $J(E^1)$ at E^1 is

$$J(E^1) = \begin{pmatrix} -\delta - \frac{a\beta\hat{P}}{(a+\hat{N})^2} & -\frac{\beta\hat{N}}{(a+\hat{N})} + \kappa\gamma & 0 \\ \frac{ae\beta\hat{P}}{(a+\hat{N})^2} - \gamma & \frac{e\beta\hat{N}}{(a+\hat{N})} - \gamma & -C(\hat{P}) \\ 0 & 0 & mC(\hat{P}) - \eta \end{pmatrix}.$$

The two eigenvalues of $J(E^1)$ satisfy the following relations:

$$\lambda_1 + \lambda_2 = -\delta - \frac{a\beta\hat{P}}{(a+\hat{N})^2} + \frac{e\beta\hat{N}}{(a+\hat{N})} - \gamma$$

and

$$\lambda_1\lambda_2 = \frac{ae\beta^2\hat{N}\hat{P}}{(a+\hat{N})^3} + \left(\gamma - \frac{e\beta\hat{N}}{(a+\hat{N})}\right)\left(\delta + \frac{a\beta\hat{P}}{(a+\hat{N})^2}\right).$$

If

$$\gamma > \frac{e\beta\hat{N}}{(a+\hat{N})}, \tag{3}$$

then we obtained that $\lambda_1 + \lambda_2 < 0$ and $\lambda_1\lambda_2 > 0$.

Hence, by applying Routh–Hurwitz criterion λ_1 and λ_2 are negative or have negative real parts. Now, the third eigenvalue is

$$\lambda_3 = mC(\hat{P}) - \eta. \tag{4}$$

From Eq. (4) we find that the third eigenvalue is negative or positive, respectively, if $mC(\hat{P}) > \eta$ or $mC(\hat{P}) < \eta$. Thus, E^1 is LAS or unstable, provided condition (3) holds.

(iii) The interior equilibrium point $E^* = (N^*, P^*, Z^*)$ exists, and there are the positive solutions of following equations:

$$\alpha - \delta N^* - \frac{\beta N^* P^*}{a + N^*} + \kappa\gamma P^* = 0, \tag{5}$$

$$\frac{e\beta N^* P^*}{a + N^*} - C(P^*)Z^* - \gamma P^* = 0, \tag{6}$$

$$mC(P^*)Z^* - \eta Z^* = 0. \tag{7}$$

The value of P^* can be determined from Eq. (7) as

$$\begin{aligned} &\big(m + 4G_1\eta h^2 - 4G_1 mh\big)w^2 P^{*2} + (8\eta h - 4m)wG_1 P^* + 4\eta G_1 = 0, \\ &A_2 P^{*2} + A_1 P^* + A_0 = 0, \end{aligned} \tag{8}$$

where

$$A_2 = \left(G_1 mh - \frac{m}{4} - \eta G_1 h^2\right)w^2, \qquad A_1 = (m - 2\eta h)wG_1, \qquad A_0 = -\eta G_1.$$

The discriminant of Eq. (8) is $\Delta_1 = mw^2G_1(mG_1 - \eta)$. Thus, Eq. (8) has real solutions if $mG_1 > \eta$, which provides a threshold line

$$\bar{\eta}(G_1) = mG_1.$$

Equation (8) has two real solutions (provided that $A_2 \neq 0$) when $\eta < \bar{\eta}\,(= \bar{\eta}$ or $> \bar{\eta})$, which we denote by P_1 and P_2 with $P_1 < P_2$. Next, we follow the region [18]

$$\Omega = \left\{(G_1, \eta)\colon\ \frac{1}{4h} < G_1 < \frac{1}{2h},\ 0 \leqslant \eta \leqslant \bar{\eta}(G_1)\right\}.$$

For $(G_1, \eta) \in \Omega$, Eq. (8) has two solutions ($i = 1, 2$)

$$P_i^* = \frac{(m - 2\eta h)wG_1 \mp \sqrt{\Delta_1}}{2w^2(\frac{m}{4} + G_1\eta h^2 - G_1 mh)}.$$

From Eq. (5) we get

$$\delta N^{*2} - \big(\alpha - a\delta - (\beta - \kappa\gamma)P^*\big)N^* - (a\alpha + a\kappa\gamma P^*) = 0. \tag{9}$$

By Descartes' rule of signs Eq. (9) has a unique root.
Also, from Eq. (6)

$$Z^* = \frac{P^*}{C(P^*)}\left[\frac{e\beta N^*}{(a + N^*)} - \gamma\right].$$

Clearly, $Z^* > 0$ if $e\beta N^* > \gamma(a + N^*)$.

Theorem 1. *If $mG_1 > \eta$ and $\mathrm{e}\beta N^* > \gamma(a + N^*)$ holds, then $E^*(N^*, P^*, Z^*)$ of the model system* (1) *is locally asymptotically stable* (*LAS*)*, provided the following inequalities hold*:

$$\frac{C(P^*)}{P^*}Z^* < \delta + \frac{a\beta P^*}{(a + N^*)^2} + C'(P^*)Z^*, \tag{10}$$

$$\left(\frac{\beta N^*}{a + N^*} - \kappa\gamma\right)\left(\frac{ae\beta P^*}{(a + N^*)^2}\right) > \left(\delta + \frac{a\beta P^*}{(a + N^*)^2}\right)\left(\frac{C(P^*)}{P^*} - C'(P^*)\right)Z^*, \quad \textit{where } \frac{\beta N^*}{a + N^*} > \kappa\gamma, \tag{11}$$

$$A_1\rho_{11}^*\rho_{22}^* + \rho_{23}^*\rho_{22}^*\rho_{32}^* > A_1\rho_{12}^*\rho_{21}^*. \tag{12}$$

The proof is deferred to Appendix B.

Ecologically speaking, the stability of a system states that disturbance in any ecological unit does not change the system dynamics. With the help of parametric set as mentioned in Table 1, we get the numeric value of E^* as $E^*(N^*, P^*, Z^*) = (4.8989, 0.4705, 1.9619)$ for the model system (1), which shows interior equilibrium point is stable. Also,

we check conditions (10)–(12) numerically and found the following:

(i) $\dfrac{C(P^*)}{P^*}Z^* = 0.8339 < 1.5143 = \delta + \dfrac{a\beta P^*}{(a+N^*)^2} + C'(P^*)Z^*;$

(ii) $\left(\dfrac{\beta N^*}{a+N^*} - \kappa\gamma\right)\dfrac{ae\beta P^*}{(a+N^*)^2}$
$= 0.1072 > 0.0197 = \left(\delta + \dfrac{a\beta P^*}{(a+N^*)^2}\right)\left(\dfrac{C(P^*)}{P^*} - C'(P^*)\right)Z^*,$
where $\beta N^*/(a+N^*) = 1.6440 > 0.5600 = \kappa\gamma;$

(iii) $A_1\rho_{11}^*\rho_{22}^* + \rho_{23}^*\rho_{22}^*\rho_{32}^* = -0.0203 > -0.0720 = A_1\rho_{12}^*\rho_{21}^*$
$\Longrightarrow \quad E^*(N^*, P^*, Z^*) = (4.8989, 0.4705, 1.9619)$ is LAS.

4 Analysis and biological interpreation of delay-induced model system

Applying Theorem 3.4 in Chapter 3 of the book by Hal Smith [26], we can obtain that the solutions of system (2) with the initial conditions $(\phi_1, \phi_2, \phi_3) \in C([-\tau, 0], \mathbb{R}^3_+)$ are nonnegative. Then the feasible region of the model (2) can be obtained.

Now, to analyze the local stability criteria of the delayed model system (2), we perturb the system about $E^*(N^*, P^*, Z^*)$ as $N^* = N(t) - \bar{U}(t)$, $P^* = P(t) - \bar{V}(t)$, $Z^* = Z(t) - \bar{W}(t)$ and get the new linearized system of equations as

$$\begin{aligned}
\frac{\mathrm{d}\bar{U}}{\mathrm{d}t} &= p_{100}\bar{U} + p_{010}\bar{V} + \bar{p}_{010}\bar{V}(t-\tau),\\
\frac{\mathrm{d}\bar{V}}{\mathrm{d}t} &= q_{100}\bar{U} + q_{010}\bar{V} + q_{001}\bar{W},\\
\frac{\mathrm{d}\bar{W}}{\mathrm{d}t} &= r_{010}\bar{V},
\end{aligned} \tag{13}$$

where

$$\begin{gathered}
p_{100} = -\delta - \frac{a\beta P^*}{(a+N^*)^2}, \qquad p_{010} = -\frac{\beta N^*}{a+N^*}, \qquad \bar{p}_{010} = \kappa\gamma,\\
q_{100} = \frac{ae\beta P^*}{(a+N*)^2}, \qquad q_{010} = \left(\frac{C(P^*)}{P^*} - C'(P^*)\right)Z^*,\\
q_{001} = -C(P^*), \qquad r_{010} = mC'(P^*)Z^*.
\end{gathered}$$

The characteristics equation of system (13) is

$$\lambda^3 + \beta_2\lambda^2 + \beta_1\lambda + \beta_0 + \mathrm{e}^{-\lambda\tau}(\gamma_1\lambda) = 0, \tag{14}$$

where

$$\begin{gathered}
\beta_2 = -(p_{100} + q_{010}), \qquad \beta_1 = \big(p_{100}q_{010} - (q_{001}r_{010} + p_{010}q_{100})\big),\\
\beta_0 = p_{100}q_{001}r_{010}, \qquad \gamma = -q_{100}\bar{p}_{010}.
\end{gathered}$$

If $\tau = 0$ in Eq. (14), we get the characteristic equation of delay-free system, which is same as given by Eq. (B.1). Hence, we omit it.

Suppose that for some $\tau \neq 0$, $\lambda = \pm \mathrm{i}\omega$ is a pair of purely imaginary roots of the characteristic Eq. (14), then ω must satisfy

$$-\mathrm{i}\omega^3 - \beta_2\omega^2 + \mathrm{i}\beta_1\omega + \beta_0 + \mathrm{i}\gamma_1\omega\cos\omega\tau + \gamma_1\omega\sin\omega\tau = 0.$$

Simplifying the above equation gives us

$$\begin{aligned} -\beta_2\omega^2 + \beta_0 &= -\gamma_1\omega\sin\omega\tau, \\ -\omega^3 + \beta_1\omega &= -\gamma_1\omega\cos\omega\tau. \end{aligned} \tag{15}$$

Now, squaring and adding Eqs. (15), we get

$$\omega^6 + \big(\beta_2^2 - 2\beta_1\big)\omega^4 + \big(\beta_1^2 - 2\beta_2\beta_0 - \gamma_1^2\big)\omega^2 + \beta_0^2 = 0.$$

Let $v = \omega^2$, this leads the following cubic equation in terms of v:

$$v^3 + q_2v^2 + q_1v + q_0 = 0,$$

where

$$q_2 = \big(\beta_2^2 - 2\beta_1\big), \qquad q_1 = \big(\beta_1^2 - 2\beta_2\beta_0 - \gamma_1^2\big), \qquad q_0 = \beta_0^2.$$

For the roots distribution, let

$$H(v) = v^3 + q_2v^2 + q_1v + q_0, \tag{16}$$

then

$$H'(v) = 3v^2 + 2q_2v + q_1.$$

The roots of $H'(v) = 0$ can be expressed as

$$v_1^* = \frac{-q_2 + \sqrt{q_2^2 - 3q_1}}{3}, \qquad v_2^* = \frac{-q_2 - \sqrt{q_2^2 - 3q_1}}{3}.$$

We will assume the following hypothesis:

(H1) $q_2 < 0$, $q_2^2 - 3q_1 > 0$ and $H(v_1^*) < 0$.

Since $q_0 > 0$, Eq. (16) has no real positive roots if $q_2^2 - 3q_1 < 0$ and two real positive roots if (H1) holds, and these roots will be v_j $(j = 1, 2)$. Let $v_1 < v_2$, then $H'(v_1) < 0$ and $H'(v_2) > 0$.

Putting $\omega_j = \sqrt{v_j}$ $(j = 1, 2)$ in Eq. (15), we have

$$\tau_j^k = \frac{1}{\omega_j}(\theta_j + 2k\pi), \quad j = 1, 2;\ k = 0, 1, 2, \ldots,$$

where $\theta_j \in (0, 2\pi]$ satisfies $\sin\theta_j = (\beta_2\omega_j^2 - \beta_0)/(\gamma_1\omega_j)$, $\cos\theta_j = (\omega_j^2 - \beta_1)/\gamma_1$.

Then $\pm\mathrm{i}\omega_j$ is a pair of purely imaginary roots of Eq. (14) with τ_j^k, $j = 1, 2$; $k = 0, 1, 2, \ldots$, and Hopf bifurcation occurs.

Now, let us define $\tau^* = \tau_{j_0}^{(0)} = \min_{1\leqslant j\leqslant 2}\{\tau_j^{(0)}\}$ and $\omega^* = \omega_{j_0}$. In this section, we analyze the local stability criteria of the model system (2).

Lemma 2. *If* (H1) *holds and* $\omega_j^2 = v_j$ *for* $j = 1, 2$, *then we have the following two transversality conditions*:

$$\left[\frac{\mathrm{d}(\operatorname{Re}\lambda(\tau))}{\mathrm{d}\tau}\right]_{\tau=\tau_1^k,} > 0 \quad \textit{and} \quad \left[\frac{\mathrm{d}(\operatorname{Re}\lambda(\tau))}{\mathrm{d}\tau}\right]_{\tau=\tau_2^k,} < 0 \quad (k = 0, 1, 2, \dots).$$

Proof. Differentiating the characteristic equation (14) with respect to τ, we obtain

$$\left[\frac{\mathrm{d}\lambda}{\mathrm{d}\tau}\right]^{-1} = -\frac{(3\lambda^2 + 2\beta_2\lambda + \beta_1)}{\lambda(\lambda^3 + \beta_2\lambda^2 + \beta_1\lambda + \beta_0)} + \frac{\gamma_1}{\gamma_1\lambda^2} - \frac{\tau}{\lambda}. \tag{17}$$

Now, substituting $\lambda(\tau) = \varphi(\tau) + \mathrm{i}\omega(\tau)$ in Eq. (17) such that $\varphi(\tau_j^k) = 0$ and $\omega(\tau_j^k) = \omega_j(\tau_j^k)$, we obtain

$$\left[\frac{\mathrm{d}\operatorname{Re}\lambda(\tau)}{\mathrm{d}\tau}\right]^{-1}_{\tau=\tau_j^k} = \frac{\omega_j^2}{\Lambda_1}\left[3\omega_j^4 + 2\left(\beta_2^2 - 2\beta_1\right)\omega_j^2 + \left(\beta_1^2 - 2\beta_2\beta_0 - \gamma_1^2\right)\right] = \frac{\omega_j^2}{\Lambda_1}H'\left(\omega_j^2\right),$$

$$\begin{aligned}\Lambda_1 = {} & \left(\beta_1 - 3\omega_j^2 + \gamma_1\cos\omega_j\tau_j^k - \gamma_1\omega_j\tau_j^k\sin\omega_j\tau_j^k\right)^2 \\ & + \left(2\beta_2\omega_j - \gamma_1\sin\omega_j\tau_j^k - \gamma_1\omega_j\tau_j^k\cos\omega_j\tau_j^k\right)^2.\end{aligned}$$

As $\omega_j^2 = v_j$, this implies

$$\left[\frac{\mathrm{d}\operatorname{Re}\lambda(\tau)}{\mathrm{d}\tau}\right]^{-1}_{\tau=\tau_j^k} = \frac{\omega_j^2}{\Lambda_1}H'(v_j).$$

If $v_1 < v_2$, then $H'(v_1) < 0$ and $H'(v_2) > 0$. □

The stability criteria in absence of delay is no longer enough to guarantee the stability in the presence of delay, rather there is a value of time lag τ^* such that the system is stable for $\tau < \tau^*$ and become unstable for $\tau > \tau^*$. Biologically, it shows that all the species coexist and exhibit oscillatory behaviour.

5 Properties of bifurcating periodic solutions

In this section, we discuss the properties of bifurcating periodic solutions of system (2) about $E^*(N^*, P^*, Z^*)$ based on the numerical approach described by Hassard et al. [13]. We calculate (for the detailed calculation, see Appendix C)

$$\begin{aligned}g_{20} = {} & 2\tau^*\overline{M}\left[(\sigma_2 p_{110} + p_{200}) + \overline{\sigma}_2^*\left(\sigma_2 q_{110} + \sigma_2\sigma_3 q_{011} + q_{200} + \sigma_2^2 q_{020}\right)\right. \\ & \left. + \overline{\sigma}_3^*\left(\sigma_2\sigma_3 r_{011} + \sigma_2^2 r_{020}\right)\right], \\ g_{11} = {} & 2\tau^*\overline{M}\left[\left(\operatorname{Re}(\sigma_2)p_{110} + p_{200}\right)\right. \\ & + \overline{\sigma}_2^*\left(\operatorname{Re}(\sigma_2)q_{110} + \operatorname{Re}(\sigma_2\overline{\sigma}_3)q_{011} + q_{200} + \sigma_2\overline{\sigma}_2 q_{020}\right) \\ & \left. + \overline{\sigma}_3^*\left(\operatorname{Re}(\sigma_2\overline{\sigma}_3)r_{011} + \sigma_2\overline{\sigma}_2 r_{020}\right)\right], \\ g_{02} = {} & 2\tau^*\overline{M}\left[(\overline{\sigma}_2 p_{110} + p_{200}) + \overline{\sigma}_2^*\left(\overline{\sigma}_2 q_{110} + \overline{\sigma}_2\overline{\sigma}_3 q_{011} + q_{200} + \overline{\sigma}_2^2 q_{020}\right)\right. \\ & \left. + \overline{\sigma}_3^*\left(\overline{\sigma}_2\overline{\sigma}_3 r_{011} + \overline{\sigma}_2^2 r_{020}\right)\right],\end{aligned}$$

$$
\begin{aligned}
g_{21} = {} & 2\tau^*\overline{M}\Bigg[p_{110}\bigg(W_{11}^{(2)}(0)+\frac{1}{2}W_{20}^{(2)}(0)+\frac{1}{2}\overline{\sigma}_2W_{20}^{(1)}(0)+\sigma_2W_{11}^{(1)}(0)\bigg)\\
& + p_{200}\big(W_{20}^{(1)}(0)+2W_{11}^{(1)}(0)\big)\\
& + \overline{\sigma}_2^*\bigg(q_{110}\bigg(W_{11}^{(2)}(0)+\frac{1}{2}W_{20}^{(2)}(0)+\frac{1}{2}\overline{\sigma}_2W_{20}^{(1)}(0)+\sigma_2W_{11}^{(1)}(0)\bigg)\\
& + q_{011}\bigg(\sigma_2W_{11}^{(3)}(0)+\overline{\sigma}_2\frac{1}{2}W_{20}^{(3)}(0)+\overline{\sigma}_3\frac{1}{2}W_{20}^{(2)}(0)+\sigma_3W_{11}^{(2)}(0)\bigg)\\
& + q_{200}\big(W_{20}^{(1)}(0)+2W_{11}^{(1)}(0)\big)+q_{020}\big(\overline{\sigma}_2W_{20}^{(2)}(0)+2\sigma_2W_{11}^{(2)}(0)\big)\bigg)\\
& + \overline{\sigma}_3^*\bigg(r_{011}\bigg(\sigma_2W_{11}^{(3)}(0)+\overline{\sigma}_2\frac{1}{2}W_{20}^{(3)}(0)+\overline{\sigma}_3\frac{1}{2}W_{20}^{(2)}(0)+\sigma_3W_{11}^{(2)}(0)\bigg)\\
& + r_{020}\big(\overline{\sigma}_2W_{20}^{(2)}(0)+2\sigma_2W_{11}^{(2)}(0)\big)\bigg)\Bigg]. \qquad (18)
\end{aligned}
$$

Hence, the following values can be calculated:

$$
\begin{aligned}
c_1(0) &= \frac{\mathrm{i}}{2\omega^*\tau^*}\bigg(g_{20}g_{11}-2|g_{11}|^2-\frac{|g_{02}|^2}{3}\bigg)+\frac{g_{21}}{2}, \qquad \mu_2 = -\frac{\operatorname{Re}\{c_1(0)\}}{\operatorname{Re}\{\lambda'(\tau^*)\}},\\
\beta_2 &= 2\operatorname{Re}\big\{c_1(0)\big\}, \qquad T_2 = -\frac{\operatorname{Im}\{c_1(0)\}+\mu_2\operatorname{Im}\{\lambda'(\tau^*)\}}{\omega^*\tau^*}.
\end{aligned} \qquad (19)
$$

The values of Eq. (19) are used to determine the bifurcating periodic solution in the center manifold at the critical value τ^*.

Theorem 2. *From Eq.* (19) *the following results have been obtained*:

(i) *Direction of the Hopf bifurcation is forward* (*backward*) *if* $\mu_2 > 0$ ($\mu_2 < 0$).
(ii) *Bifurcating periodic solution is stable* (*unstable*) *if* $\beta_2 < 0$ ($\beta_2 > 0$).
(iii) *Period of the bifurcating periodic solution increases* (*decreases*) *if* $T_2 > 0$ ($T_2 < 0$).

We examined the criterion for double-Hopf bifurcation (forward and backward) on the stability of model system.

6 Numerical experiments

The numerical experiments are performed to observe the role of parameters and compare the changes in system dynamics. Here, we have performed the numerical computations to validate our analytical outcomes and also made an attempt to understand the possible dynamics of delay-induced nutrient–plankton system with TDFR. In order to grasp the implications of some key parameters, we plotted various bifurcation diagrams under various situations corresponding to systems (1) and (2). Further, to study how delay-induced nutrient recycling influences the system dynamics, we consider the combined effect of time delay and various nutrient levels. With this intent, we considered the

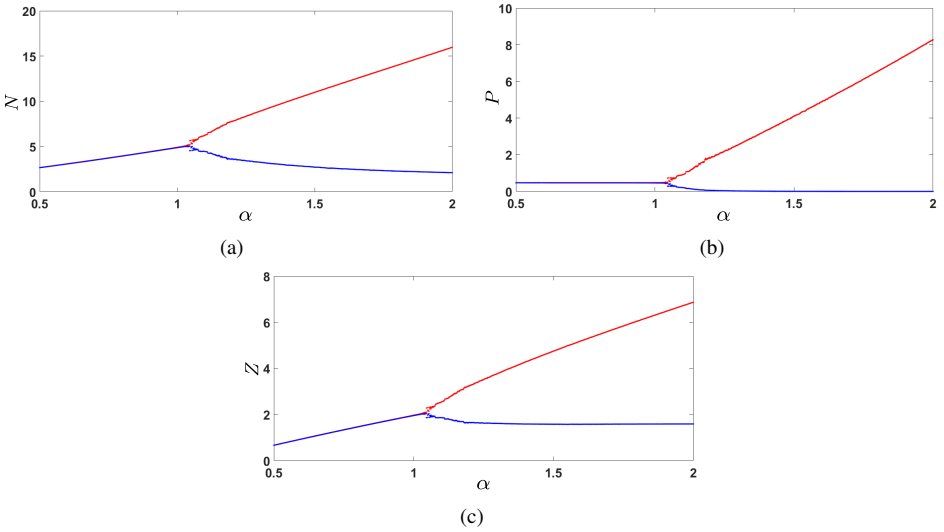

Figure 2. Bifurcation diagram of the model system (1) with varying input concentration of nutrients α vs. population densities.

parametric values as given in Table 1. The system has two crucial parameters, i.e., the input concentration of nutrients α and the removal rate of nutrients δ, and with respect to these parameters, the major dynamical changes of the model systems (1) and (2) has tried to identify. In Fig. 2, we have plotted the bifurcation diagram by taking α as a bifurcation parameter, and rest parameter values are given in Table 1. From Fig. 2 we noticed the max-min plot of nutrient, phytoplankton, and zooplankton in the intervals $0 \leqslant N \leqslant 20$, $0 \leqslant P \leqslant 10$, and $0 \leqslant Z \leqslant 8$, respectively, as α is considered in the interval $0.5 \leqslant \alpha \leqslant 2$. Here, the max-min limits of the oscillations are represented by red and blue lines, respectively. Under the bifurcation analysis, stable focus is observed in the range $0.5 \leqslant \alpha \leqslant 1.051$, and after crossing the critical values of $\alpha = \alpha_{\mathrm{cr}} = 1.051$, oscillatory behavior is observed. Further, to analyze the effect of the removal rate of nutrients δ for the model system (1), we have plotted bifurcation diagram by taking δ as bifurcation parameter in the range $0.0 \leqslant \delta \leqslant 0.2$, where the maxi-min limits of the oscillations are represented by red and blue lines, respectively (c.f., Fig. 3). From Figs. 2 and 3 it has been noticed that some parametric manipulations can stabilize as well as destabilize the nutrient–plankton system (1).

In order to study the impact of delay induced nutrient recycling on the dynamics of nutrient–plankton system (2), we have simulated the system's behavior for varying τ with different fixed values of input concentration of nutrients α by the representation of time series, phase space, and bifurcation diagrams. We have noticed that the interior equilibrium point E^* is locally asymptotically stable at $\alpha = 1$ and $\tau = 0$. For fixed $\alpha = 1$, we have plotted the bifurcation diagrams by taking τ as a bifurcation parameter. From Fig. 4(a) we noticed the max-min plot of nutrient–plankton system in the interval $[0, 12]$ as τ is considered in the interval $0 \leqslant \tau \leqslant 14$. By some computation we obtained the critical value of τ as $\tau = \tau^* = 7.15$, which shows the Hopf-bifurcation scenario

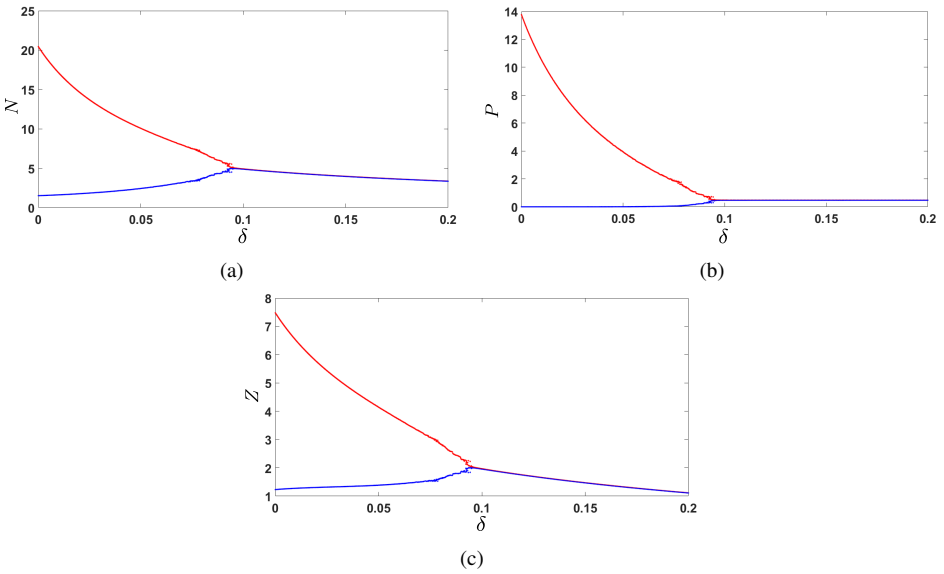

(a) (b) (c)

Figure 3. Bifurcation diagram of the model system (1) with varying removal rate of nutrients δ vs. population densities.

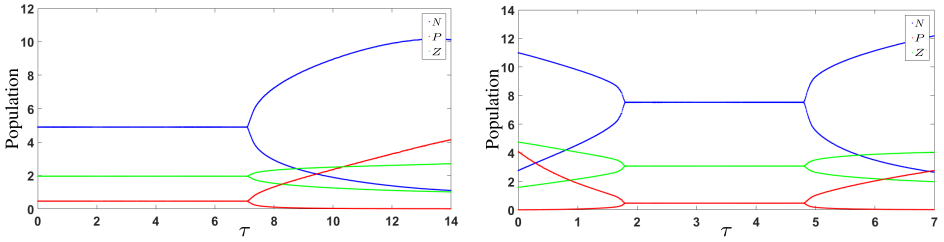

(a) $\alpha = 1$ (b) $\alpha = 1.5$

Figure 4. Bifurcation diagram of the model system (2) with varying delay parameter τ for fixed α.

corresponding to τ. The Hopf-bifurcation scenario in Fig. 4(a) revealed that the system bifurcates around $\tau = \tau^* = 7.15$, and stable interior equilibrium becomes unstable. By time series and phase space diagram we have shown that system shows a stable behavior for $\tau = 6$ and limit cycle behavior for $\tau = 8$ (c.f., Fig. 5). Again, we noticed a limit cycle behavior at $\alpha = 1.5$ and $\tau = 0$. For fixed $\alpha = 1.5$, we have plotted the bifurcation diagrams by taking τ as a bifurcation parameter. From Fig. 4(b) we noticed the max-min plot of nutrient–plankton system in the interval $[0, 14]$ as τ is considered in the interval $0 \leqslant \tau \leqslant 7$. This result indicates that the nutrient recycling delay τ with fixed $\alpha = 1.5$ supports the existence of Hopf bifurcation (i.e., double-Hopf bifurcation) for system (2). Therefore, model system contains two critical values of τ, the first one is $\tau = \tau_1^* = 1.85$, and the second one is $\tau = \tau_2^* = 4.90$. Time series diagram for this phenomenon for various values of τ is given in Fig. 6, which shows that a periodic solution becomes stable

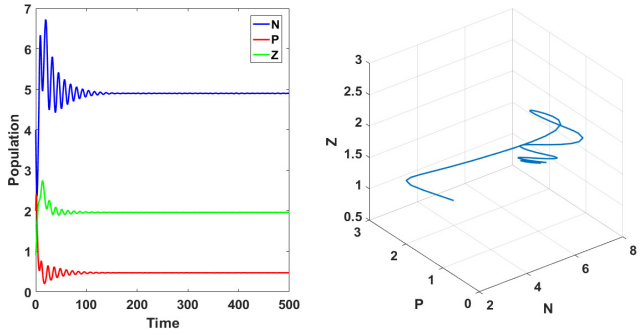

(a) $\tau = 6 < \tau^*$

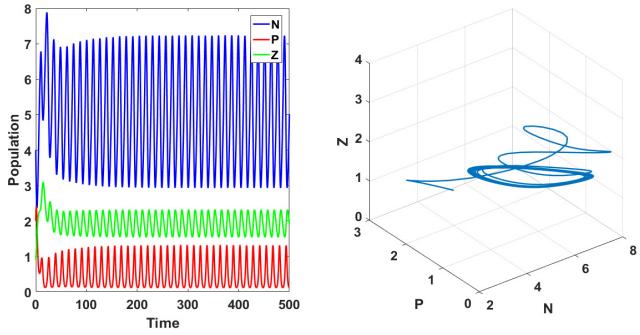

(b) $\tau = 8 > \tau^*$

Figure 5. Time series and phase space diagram of the model system (2) with fixed $\alpha = 1$.

in nature when the system crosses τ_1^*, and after that, a stable solution becomes again periodic in nature when the system crosses τ_2^*.

We have drawn the parametric domain of stability and instability in Fig. 7 for input concentration of nutrients α vs. nutrient recycling delay τ to examine its vital importance on the system dynamics (2). For this purpose, we have taken $\tau \in [0, 14]$ in vertical axis and vary the input concentration of nutrients $\alpha \in [0.5, 2]$ in horizontal axis. The entire domain has been divided into three subdomains (two blue domains and one red region), viz. blue color and red color. Here the blue "$*$" indicates stable domain whereas the red "$*$" indicates unstable domain in α, τ-plane. A Hopf bifurcation occurs in the α, τ-plane when we get a critical value of τ corresponds to each α. For example, in the case of a small value of input rate of nutrients (i.e., $0.5 \leqslant \alpha \leqslant 1.051$), the system switches its behavior from stable to unstable and produces oscillation cycles for a sufficiently large value of time delay τ. Moreover, the higher input rate of nutrients along with time delay (about $\alpha = 1.5$) shows stability switching phenomenon along with the time delay. Further, it can also show the Hopf-bifurcation phenomenon along with the time delay. The transition line that separated the region into blue and red, is known as Hopf-bifurcation line of system (2).

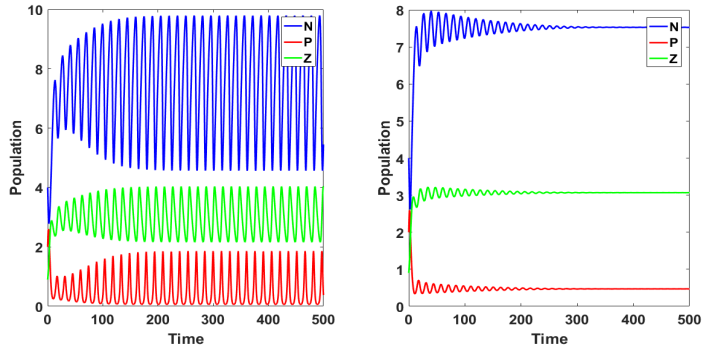

(a) $\tau = 1 < \tau_1^*$ (b) $\tau = 2.25 > \tau_1^*$

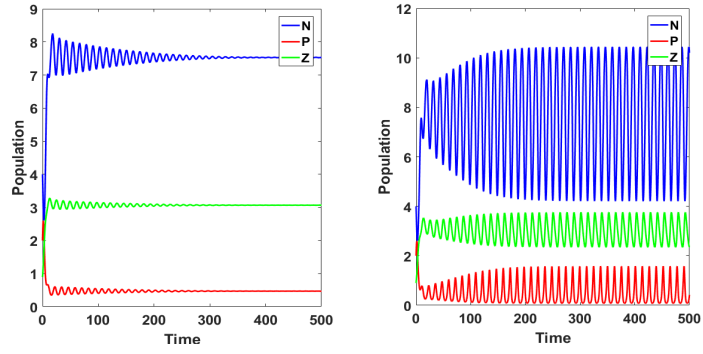

(c) $\tau = 4.5 < \tau_2^*$ (d) $\tau = 5.5 > \tau_2^*$

Figure 6. Time series of the model system (2) with fixed $\alpha = 1.5$.

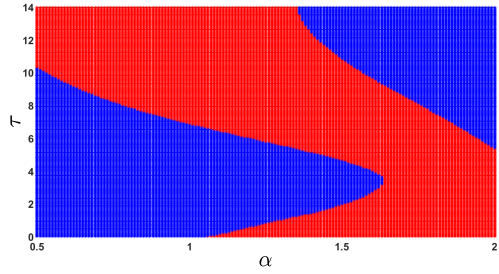

Figure 7. The effect of α and τ on the system dynamics (2).

We have noticed a limit cycle behavior at $\delta = 0.05$ and $\tau = 0$. For fixed $\delta = 0.05$, we have observed in the bifurcation diagrams by taking τ as a bifurcation parameter and rest parameter values are given in Table 1. We noticed in the max-min plot of nutrient–plankton system in the interval $[0, 20]$ as τ is considered in the interval $0 \leqslant \tau \leqslant 30$. This observation indicates that the nutrient recycling delay τ with fixed $\delta = 0.05$ can induce the stability switches of positive equilibrium. Using the set of parameters as given

in Table 1, we get the value of $c_1(0) = -0.1175 - 2.7969\mathrm{i}$ at $\tau = \tau^* = 7.15$. Thus, $\mathrm{Re}\{c_1(0)\} = -0.1175$.

7 Discussion and conclusion

Sundarban is one of the largest mangrove wetland that forms an estuarine phase with the Ganga–Brahmaputra river system. The uncontrolled growth of phytoplankton (microalgae) has posed a threat to the rich biodiversity of Sundarban that have deteriorated the water quality and declined the fish population. Das and Ray [9] have studied the phytoplankton–zooplankton interactions with delayed nutrient cycling from senescence and mortality of phytoplankton in Hooghly–Matla estuarine system and determined how the nutrients are regulated by the phytoplankton loss due to senescence and other deaths and also to know the effects of delay on the decomposition process of dead phytoplankton. Lui et al. [18] examined a two-dimensional plant–herbivore interactions model mediated by a TDFR and observed the complex dynamics, which have important biological implications for the plant–herbivore interaction under the influence of plant toxicity. Further, Chatterjee and Pal [5] proposed and analysed a three-dimensional plankton–nutrient interaction model, which mediated by a TDFR. They have found that constant nutrient input and dilution rate of nutrient influence the plankton ecosystem and maintain stability around the coexistence equilibrium, and their observations indicate that if the constant nutrient input crosses a certain critical value, the system enters into Hopf bifurcation. Keeping these things in view, we have attempted to examine the role of delay-induced nutrient recycling with TDFR in the interacting nutrient–plankton system of Sundarban estuarine to extend the series of works [5, 9, 18, 32]. We have hybridized two different response functions for the proposed model system. We have assumed that nutrient is always available in abundant amount in the estuarine due to sewage dispose and wastewater discharges, and nutrient consumption has no limit. The plankton interaction modelled with the TDFR shows the zooplankton density is severely affected by toxicity released by phytoplankton. In general, the reconversion process of nutrients must take some time lag. Therefore, a nutrient recycling time delay incorporates into the system due to the decomposition of dead biomass of phytoplankton. The effect of some other crucial parameters of the model system is also studied explicitly. Theoretically, we have established that system (1) is bounded under certain conditions that ensure the biological feasibility of the model system. We have also investigated all the existing equilibrium points and observed the system's local stability behavior around them. Note that the system does not have any trivial equilibrium point. Numerically, we have studied the system dynamics with and without delay and observed various excitable dynamics, including the stable and periodic solutions via Hopf and double-Hopf bifurcation. For delay-free system, the results indicate that the system is affected by input concentration of nutrients α and removal rate of nutrients δ (c.f., Figs. 2 and 3). A simple Hopf-bifurcation scenario is observed for all these two parameters when they cross their critical values. We found that the input concentration of nutrients has essential consequences on nutrient and the growth of zooplankton as the decreasing value of

α decreases their densities (c.f., Fig. 2). In Fig. 3, extinction scenario is observed for zooplankton density for a higher value of the removal rate of nutrients δ. Biologically, a higher removal rate of nutrients may be one reason for the extinction of the plankton community.

The most important finding is the effect of time delay in the decomposition process of phytoplankton and nutrient input concentration α on the system dynamics. For the model system (2), stable solution has been noticed for $\alpha = 1$ and $\tau = 0$. Further, taking the value of $\tau > 0$ for fixed $\alpha = 1$, the system's solution trajectories converge stable to oscillatory solution and all the population bifurcates around the critical value of $\tau = \tau^* = 7.15$ (c.f., Fig. 4(a)). We have obtained the limit cycle behavior at $\alpha = 1.5$ and $\tau = 0$. The bifurcation diagrams are plotted for varying τ and fixed $\alpha = 1.5$ in Fig. 4(b). Double-Hopf critical points are obtained in this bifurcation analysis. In Fig. 6, time series diagram for various values of τ are shown for fixed $\alpha = 1.5$. Our observation revealed that the occurrence of Hopf and double-Hopf bifurcation of the nutrient–plankton system mainly depends on two crucial parameters: (i) input concentration of nutrient α and (ii) time delay τ. It regulates the system dynamics and has the potential to make the system stable to unstable and vice versa. We have observed stability switching with increasing time delay for the model system (2) with fixed $\delta = 0.05$. Our study may be helpful to predict the impact of time delay in nutrient recycling and input concentration of nutrients for the wetland ecosystem. Furthermore, we did not consider the delayed diffusion of nutrients, phytoplankton, and zooplankton; therefore, these aspects should be considered comprehensively in our future research.

Appendix A

Let us consider a function

$$W(t) = N(t) + \frac{1}{e}P(t) + \frac{1}{em}Z(t). \tag{A.1}$$

Differentiating Eq. (A.1) with respect to t, we get

$$\frac{\mathrm{d}W}{\mathrm{d}t} = \frac{\mathrm{d}N}{\mathrm{d}t} + \frac{1}{e}\frac{\mathrm{d}P}{\mathrm{d}t} + \frac{1}{em}\frac{\mathrm{d}Z}{\mathrm{d}t}.$$

Now, using Eq. (1) under the condition as $\xi > 0$, we have

$$\begin{aligned}\frac{\mathrm{d}W}{\mathrm{d}t} + \xi W &= \left(\alpha - \delta N - \frac{\beta NP}{a+N} + \kappa\gamma P\right) + \frac{1}{e}\left(\frac{e\beta NP}{a+N} - C(P)Z - \gamma P\right)\\ &\quad + \frac{1}{em}\big(mC(P)Z - \eta Z\big) + \xi W,\\ &= \alpha - (\delta - \xi)N - \frac{1}{e}\big((1-\kappa)\gamma - \xi\big)P - \frac{1}{em}(\eta - \xi)Z,\\ &\leqslant \alpha - (\delta - \xi)N - \frac{1}{e}\big((1-\kappa)\gamma - \xi\big)P - \frac{1}{em}(\eta - \xi)Z.\end{aligned}$$

Defining $\xi = \min(\delta, (1-\kappa)\gamma, \eta)$, we can find $\alpha > 0$ such that $\mathrm{d}W/\mathrm{d}t + \xi W \leqslant \alpha$, which implies that

$$W(t) \leqslant \frac{\alpha}{\xi} + \left(W(0) - \frac{\alpha}{\xi}\right)\mathrm{e}^{-\xi t}.$$

This implies, $\limsup_{t\to\infty} W(t) \leqslant \alpha/\xi$. Thus,

$$W(t) = N(t) + \frac{1}{e}P(t) + \frac{1}{em}Z(t) \leqslant \frac{\alpha}{\xi}.$$

System (1) is uniformly bounded.

Appendix B

The variational matrix $J(E^*)$ at E^* is

$$J(E^*) = \begin{pmatrix} \rho_{11}^* & \rho_{12}^* & \rho_{13}^* \\ \rho_{21}^* & \rho_{22}^* & \rho_{23}^* \\ \rho_{31}^* & \rho_{32}^* & \rho_{33}^* \end{pmatrix},$$

where

$$\rho_{11}^* = -\delta - \frac{a\beta P^*}{(a+N^*)^2}, \qquad \rho_{12}^* = -\left(\frac{\beta N^*}{a+N^*} - \kappa\gamma\right), \qquad \rho_{13}^* = 0,$$
$$\rho_{21}^* = \frac{ae\beta P^*}{(a+N*)^2}, \qquad \rho_{22}^* = \left(\frac{C(P^*)}{P^*} - C'(P^*)\right)Z^*, \qquad \rho_{23}^* = -C(P^*),$$
$$\rho_{31}^* = 0, \qquad \rho_{32}^* = mC'(P^*)Z^*, \qquad \rho_{33}^* = 0.$$

The characteristics equation about $E^*(N^*, P^*, Z^*)$ is given by

$$\upsilon^3 + A_1\upsilon^2 + A_2\upsilon + A_3 = 0, \tag{B.1}$$

where

$$A_1 = -(\rho_{11}^* + \rho_{22}^*), \qquad A_2 = (\rho_{11}^*\rho_{22}^* - \rho_{12}^*\rho_{21}^*) - \rho_{23}^*\rho_{32}^*, \qquad A_3 = \rho_{11}^*\rho_{23}^*\rho_{32}^*,$$
$$A_1A_2 - A_3 = A_1(\rho_{11}^*\rho_{22}^* - \rho_{12}^*\rho_{21}^*) + \rho_{32}^*\rho_{23}^*\rho_{22}^*.$$

By Routh–Hurwitz criteria we obtained Theorem 1.

Appendix C

Let $N = N^* + \eta_1$, $P = P^* + \eta_2$, $Z = Z^* + \eta_3$, $\upsilon = \tau - \tau^*$, where $\upsilon \in \mathbb{R}$ and at $\upsilon = 0$ gives the value of Hopf bifurcation. Rescaling the time by $t \to t/\tau$, system (2) can be written into the following continuous real-valued functions in $C = ([-1, 0], \mathbb{R}^3)$:

$$\dot{\eta}(t) = L_\upsilon(\eta_t) + F(\upsilon, \eta_t),$$

where $x(t) = (\eta_1(t), \eta_2(t), \eta_3(t))^{\mathrm{T}} \in \mathbb{R}^3$, and $L_\upsilon : C \to \mathbb{R}^3$, $F : \mathbb{R} \times C \to \mathbb{R}^3$ are given, respectively,

$$L_\upsilon(\phi) = (\tau^* + \upsilon)\big[V_1\phi(0) + V_2\phi(-1)\big],$$

where

$$V_1 = \begin{pmatrix} p_{100} & p_{010} & 0 \\ q_{100} & q_{010} & q_{001} \\ 0 & r_{010} & 0 \end{pmatrix} = \begin{pmatrix} -\delta - \frac{a\beta P^*}{(a+N^*)^2} & -\frac{\beta N^*}{a+N^*} & 0 \\ \frac{ae\beta P^*}{(a+N*)^2} & \left(\frac{C(P^*)}{P^*} - C'(P^*)\right)Z^* & -C(P^*) \\ 0 & mC'(P^*)Z^* & 0 \end{pmatrix},$$

$$V_2 = \begin{pmatrix} 0 & \bar{p}_{010} & 0 \\ 0 & 0 & 0 \\ 0 & 0 & 0 \end{pmatrix} = \begin{pmatrix} 0 & \kappa\gamma & 0 \\ 0 & 0 & 0 \\ 0 & 0 & 0 \end{pmatrix},$$

and

$$F(\upsilon, \phi) = (\tau^* + \upsilon) \begin{pmatrix} p_{110}\phi_1(0)\phi_2(0) + p_{200}\phi_1^2(0) \\ q_{110}\phi_1(0)\phi_2(0) + q_{011}\phi_2(0)\phi_3(0) + q_{200}\phi_1^2(0) + q_{020}\phi_2^2(0) \\ r_{011}\phi_2(0)\phi_3(0) + r_{020}\phi_2^2(0) \end{pmatrix},$$

where $\phi(\theta) = (\phi_1(\theta), \phi_2(\theta), \phi_3(\theta))^{\mathrm{T}} \in C([-1, 0], \mathbb{R}^3)$, and

$$p_{110} = -\frac{a\beta}{(a+N^*)^2}, \qquad p_{200} = -\frac{2a\beta P^*}{(a+N^*)^3},$$

$$q_{110} = -\frac{ae\beta}{(a+N^*)^2}, \qquad q_{011} = \frac{C(P^*)}{P^*} - C'(P^*),$$

$$q_{200} = -\frac{2ae\beta P^*}{(a+N^*)^3}, \qquad q_{020} = \left(\frac{P^*C'(P^*) - C(P^*)}{P^{*2}} - C''(P^*)\right)Z^*,$$

$$r_{011} = mC'(P^*), \qquad r_{020} = mC''(P^*)Z^*.$$

Here, we are going to calculate some results directly by using the computational process given by [13]. Now, let $q(\theta) = (1, \sigma_2, \sigma_3)^{\mathrm{T}} \mathrm{e}^{\mathrm{i}\omega^*\tau^*\theta}$ and $q^*(s) = (1, \sigma_2^*, \sigma_3^*)\mathrm{e}^{\mathrm{i}\omega^*\tau^* s}$ be the eigenvectors of $A(0)$ and $A^*(0)$ corresponding to the eigenvalues $\mathrm{i}\omega^*\tau^*$ and $-\mathrm{i}\omega^*\tau^*$, respectively, then

$$Aq(\theta) = \mathrm{i}\omega^*\tau^* q(\theta).$$

For $\theta = 0$, we get

$$\tau^* \begin{pmatrix} \mathrm{i}\omega^* - p_{100} & -p_{010} - \bar{p}_{010}\mathrm{e}^{-\mathrm{i}\omega^*\tau^*} & 0 \\ -q_{100} & \mathrm{i}\omega^* - q_{010} & -q_{001} \\ 0 & -r_{010} & \mathrm{i}\omega^* \end{pmatrix} \cdot q(0) = \begin{pmatrix} 0 \\ 0 \\ 0 \end{pmatrix},$$

After solving the equations, we get

$$\sigma_2 = \frac{\mathrm{i}\omega^* - p_{100}}{p_{010} + \bar{p}_{010}\mathrm{e}^{-\iota\omega^*\tau^*}}, \qquad \sigma_3 = \frac{r_{010}}{\mathrm{i}\omega^*}\sigma_2.$$

Similarly, let

$$A^*q^*(s) = -\mathrm{i}\omega^*\tau^*q^*(s),$$

where

$$\sigma_2^* = -\frac{(\mathrm{i}\omega^* + p_{100})}{q_{100}}, \qquad \sigma_3^* = -\frac{q_{001}}{\mathrm{i}\omega^*}\sigma_2^*.$$

Under the normalization condition $\langle q^*(s), q(\theta)\rangle = 1$, we have $M = 1/\overline{D}$, where

$$D = 1 + \sigma_2\overline{\sigma}_2^* + \sigma_3\overline{\sigma}_3^* + \tau^*\overline{p}_{010}\sigma_2\mathrm{e}^{-\mathrm{i}\omega^*\tau^*}.$$

Now, using the algorithms described in [13], we get

$$g(z,\bar{z}) = \tau^*\overline{M}(1,\overline{\sigma}_2^*,\overline{\sigma}_3^*) \times \begin{pmatrix} p_{110}\phi_1(0)\phi_2(0) + p_{200}\phi_1^2(0) \\ (q_{110}\phi_1(0)\phi_2(0) + q_{011}\phi_2(0)\phi_3(0) + q_{200}\phi_1^2(0) + q_{020}\phi_2^2(0)) \\ r_{011}\phi_2(0)\phi_3(0) + r_{020}\phi_2^2(0) \end{pmatrix},$$

which can also be written as

$$g(z,\bar{z}) = \tau^*\overline{M}(1,\overline{\sigma}_2^*,\overline{\sigma}_3^*) \times \begin{pmatrix} p_{110}x_{1t}(0)x_{2t}(0) + p_{200}x_{1t}^2(0) \\ (q_{110}x_{1t}(0)x_{2t}(0) + q_{011}x_{2t}(0)x_{3t}(0) + q_{200}x_{1t}^2(0) + q_{020}x_{2t}^2(0)) \\ r_{011}x_{2t}(0)x_{3t}(0) + r_{020}x_{2t}^2(0) \end{pmatrix}, \quad \text{(C.1)}$$

where

$$\begin{aligned} x_{1t}(0) &= z + \bar{z} + W_{20}^{(1)}(0)\frac{z^2}{2} + W_{11}^{(1)}(0)z\bar{z} + W_{02}^{(1)}(0)\frac{\bar{z}^2}{2} + \cdots, \\ x_{2t}(0) &= \sigma_2 z + \overline{\sigma}_2\bar{z} + W_{20}^{(2)}(0)\frac{z^2}{2} + W_{11}^{(2)}(0)z\bar{z} + W_{02}^{(2)}(0)\frac{\bar{z}^2}{2} + \cdots, \\ x_{3t}(0) &= \sigma_3 z + \overline{\sigma}_3\bar{z} + W_{20}^{(3)}(0)\frac{z^2}{2} + W_{11}^{(3)}(0)z\bar{z} + W_{02}^{(3)}(0)\frac{\bar{z}^2}{2} + \cdots. \end{aligned}$$

From Eq. (C.1) we obtained the value of g_{20}, g_{11}, g_{02}, and g_{21} is given in Section 5. Now, in order to calculate g_{21}, we have to calculate the values of $W_{20}^{(l)}(\theta)$ and $W_{20}^{(l)}(\theta)$ for $l = 1, 2, 3$. Now, we denote $W_{20}(\theta) = (W_{20}^{(1)}(\theta), W_{20}^{(2)}(\theta), W_{20}^{(\theta)}(\theta))^{\mathrm{T}}$ and $W_{11}(\theta) = (W_{11}^{(1)}(\theta), W_{11}^{(2)}(\theta), W_{11}^{(3)}(\theta))^{\mathrm{T}}$.

By some calculations we get

$$W_{20}(\theta) = -\frac{g_{20}}{\mathrm{i}\omega^*\tau^*}q(\theta) - \frac{\overline{g}_{02}}{3\mathrm{i}\omega^*\tau^*}\overline{q}(\theta) + E_1\mathrm{e}^{2\mathrm{i}\omega^*\tau^*\theta}, \quad \text{(C.2)}$$

$$W_{11}(\theta) = \frac{g_{11}}{\mathrm{i}\omega^*\tau^*}q(\theta) - \frac{\overline{g}_{11}}{\mathrm{i}\omega^*\tau^*}\overline{q}(\theta) + E_2, \quad \text{(C.3)}$$

where $E_1 = (E_1^{(1)}, E_1^{(2)}, E_1^{(3)})$ and $E_2 = (E_2^{(1)}, E_2^{(2)}, E_2^{(3)}) \in \mathbb{R}^3$ are the constant vectors, which we have determined.

Applying the theory explained in [13], we get

$$E_1 = \frac{2}{M_1}\begin{pmatrix} p_{200} + \sigma_2 p_{110} \\ \sigma_2 q_{110} + \sigma_2\sigma_3 q_{011} + q_{200} + \sigma_2^2 q_{020} \\ \sigma_2\sigma_3 r_{011} + \sigma_2^2 r_{020} \end{pmatrix} = \frac{2}{M_1}\begin{pmatrix} \sigma_{11} \\ \sigma_{12} \\ \sigma_{13} \end{pmatrix}.$$

Solving the system for E_1, we obtain

$$E_1^{(1)} = \frac{2}{M_1}\begin{vmatrix} \sigma_{11} & -p_{010} - \bar{p}_{010}\mathrm{e}^{-2\mathrm{i}\omega^*\tau^*} & 0 \\ \sigma_{12} & 2\mathrm{i}\omega^* - q_{010} & -q_{001} \\ \sigma_{13} & -r_{010} & 2\mathrm{i}\omega^* \end{vmatrix},$$

$$E_1^{(2)} = \frac{2}{M_1}\begin{vmatrix} 2\mathrm{i}\omega^* - p_{100} & \sigma_{11} & 0 \\ -q_{100} & \sigma_{12} & -q_{001} \\ 0 & \sigma_{13} & 2\mathrm{i}\omega^* \end{vmatrix},$$

$$E_1^{(3)} = \frac{2}{M_1}\begin{vmatrix} 2\mathrm{i}\omega^* - p_{100} & -p_{010} - \bar{p}_{010}\mathrm{e}^{-2\mathrm{i}\omega^*\tau^*} & \sigma_{11} \\ -q_{100} & 2\mathrm{i}\omega^* - q_{010} & \sigma_{12} \\ 0 & -r_{010} & \sigma_{13} \end{vmatrix},$$

where

$$M_1 = \begin{vmatrix} 2\mathrm{i}\omega^* - p_{100} & -p_{010} - \bar{p}_{010}\mathrm{e}^{-2\mathrm{i}\omega^*\tau^*} & 0 \\ -q_{100} & 2\mathrm{i}\omega^* - q_{010} & -q_{001} \\ 0 & -r_{010} & 2\mathrm{i}\omega^* \end{vmatrix}.$$

Similarly, we have

$$E_2 = \frac{2}{M_2}\begin{pmatrix} p_{200} + \mathrm{Re}(\sigma_2)p_{110} \\ \mathrm{Re}(\sigma_2)q_{110} + \mathrm{Re}(\sigma_2\overline{\sigma}_3)q_{011} + q_{200} + \sigma_2\overline{\sigma_2}q_{020} \\ \mathrm{Re}(\sigma_2\overline{\sigma}_3)r_{011} + \sigma_2\overline{\sigma_2}r_{020} \end{pmatrix} = \frac{2}{M_2}\begin{pmatrix} \sigma_{21} \\ \sigma_{22} \\ \sigma_{23} \end{pmatrix}.$$

Solving the system for E_2, we obtain

$$E_2^{(1)} = \frac{2}{M_2}\begin{vmatrix} \sigma_{21} & -p_{010} - \bar{p}_{010} & 0 \\ \sigma_{22} & -q_{010} & -q_{001} \\ \sigma_{23} & -r_{010} & 0 \end{vmatrix}, \qquad E_2^{(2)} = \frac{2}{M_1}\begin{vmatrix} -p_{100} & \sigma_{21} & 0 \\ -q_{100} & \sigma_{22} & -q_{001} \\ 0 & \sigma_{23} & 0 \end{vmatrix},$$

$$E_2^{(3)} = \frac{2}{M_2}\begin{vmatrix} -p_{100} & -p_{010} - \bar{p}_{010} & \sigma_{21} \\ -q_{100} & -q_{010} & \sigma_{22} \\ 0 & -r_{010} & \sigma_{23} \end{vmatrix},$$

where

$$M_2 = \begin{vmatrix} -p_{100} & -p_{010} - \bar{p}_{010} & 0 \\ -q_{100} & -q_{010} & -q_{001} \\ 0 & -r_{010} & 0 \end{vmatrix}.$$

Consequently, the values of $W_{20}(\theta)$ and $W_{11}(\theta)$ are determined from Eqs. (C.2) and (C.3). The value of g_{21} is determined by delay and parameters from Eq. (18).

References

1. N. Bairagi, S. Pal, S. Chatterjee, J. Chattopadhyay, Nutrient, non-toxic phytoplankton, toxic phytoplankton and zooplankton interaction in an open marine system, in R.J. Hosking, E. Venturino (Eds.), *Aspects of Mathematical Modelling: Applications in Science, Medicine, Economics and Management*, Math. Biosci. Interac., Birkhäuser, Basel, 2008, pp. 41–63.
2. J.P. Bryant, R.K. Swihart, P.B. Reichardt, L. Newton, Biogeography of woody plant chemical defense against snowshoe hare browsing: Comparison of Alaska and eastern North America, *Oikos*, pp. 385–395, 1994, https://doi.org/https://www.jstor.org/stable/3545776.
3. S. Chakraborty, S. Chatterjee, E. Venturino, J. Chattopadhyay, Recurring plankton bloom dynamics modeled via toxin-producing phytoplankton, *J. Biol. Phys.*, **33**(4):271–290, 2007, https://doi.org/10.1007/s10867-008-9066-3.
4. S. Chakraborty, P.K. Tiwari, A.K. Misra, J. Chattopadhyay, Spatial dynamics of a nutrient–phytoplankton system with toxic effect on phytoplankton, *Math. Biosci.*, **264**:94–100, 2015, https://doi.org/10.1016/j.mbs.2015.03.010.
5. A. Chatterjee, S. Pal, Plankton nutrient interaction model with effect of toxin in presence of modified traditional Holling type II functional response, *Syst. Sci. Control Eng.*, **4**(1):20–30, 2016, https://doi.org/10.1080/21642583.2015.1136801.
6. G.H. Cui, X.P. Yan, Stability and bifurcation analysis on a three-species food chain system with two delays, *Commun. Nonlinear Sci. Numer. Simul.*, **16**(9):3704–3720, 2011, https://doi.org/10.1016/j.cnsns.2010.12.042.
7. C. Dai, H. Yu, Q. Guo, H. Liu, Q. Wang, Z. Ma, M. Zhao, Dynamics induced by delay in a nutrient-phytoplankton model with multiple delays, *Complexity*, **2019**, 2019, https://doi.org/10.1155/2019/3879626.
8. C. Dai, M. Zhao, H. Yu, Dynamics induced by delay in a nutrient–phytoplankton model with diffusion, *Ecol. Complexity*, **26**:29–36, 2016, https://doi.org/10.1016/j.ecocom.2016.03.001.
9. K. Das, S. Ray, Effect of delay on nutrient cycling in phytoplankton–zooplankton interactions in estuarine system, *Ecological Model.*, **215**(1–3):69–76, 2008, https://doi.org/10.1016/j.ecolmodel.2008.02.019.
10. A. Fan, P. Han, K. Wang, Global dynamics of a nutrient-plankton system in the water ecosystem, *Appl. Math. Comput.*, **219**(15):8269–8276, 2013, https://doi.org/10.1016/j.amc.2013.02.051.
11. Z. Feng, R. Liu, D. DeAngelis, Plant–herbivore interactions mediated by plant toxicity, *Theor. Popul. Biol.*, **73**(3):449–459, 2008, https://doi.org/10.1016/j.tpb.2007.12.004.
12. B. Gopal, M. Chauhan, Biodiversity and its conservation in the Sundarban mangrove ecosystem, *Aquat. Sci.*, **68**:338–354, 2006, https://doi.org/10.1007/s00027-006-0868-8.
13. B.D. Hassard, N.D. Kazarinoff, Y.-H. Wan, *Theory and Applications of Hopf Bifurcation*, Lond. Math. Soc. Lect. Note Ser., Vol. 41, Cambridge Univ. Press, Cambridge, 1981.

14. C.S. Holling, The components of predation as revealed by a study of small-mammal predation of the European pine sawfly, *Can. Entomol.*, **91**(5):293–320, 1959, https://doi.org/10.4039/Ent91293-5.

15. A. Huppert, B. Blasius, L. Stone, A model of phytoplankton blooms, *Am. Nat.*, **159**(2):156–171, 2002, https://doi.org/10.1086/324789.

16. J. Ji, L. Wang, Bifurcation and stability analysis for a nutrient-phytoplankton model with toxic effects, *Discrete Contin. Dyn. Syst., Ser. S*, **13**:3073–3081, 2020.

17. Y. Kuang, *Delay Differential Equations: With Applications in Population Dynamics*, Academic Press, Boston, 1993.

18. R. Liu, Z. Feng, H. Zhu, D.L. DeAngelis, Bifurcation analysis of a plant–herbivore model with toxin-determined functional response, *J. Differ. Equations*, **245**(2):442–467, 2008, https://doi.org/10.1016/j.jde.2007.10.034.

19. S. Manna, K. Chaudhuri, S. Bhattacharyya, M. Bhattacharyya, Dynamics of Sundarban estuarine ecosystem: Eutrophication induced threat to mangroves, *Aquat. Biosyst.*, **6**:8, 2010, https://doi.org/10.1186/1746-1448-6-8.

20. D. Mukherjee, S. Ray, D. Sinha, Bifurcation analysis of a detritus-based ecosystem with time delay, *J. Biol. Syst.*, **8**(03):255–261, 2000, https://doi.org/10.1142/S0218339000000183.

21. A. Ojha, N.K. Thakur, Delay-induced Hopf and double Hopf-bifurcation in plankton system with dormancy of predators, *Nonlinear Dyn.*, **105**(1):997–1018, 2021, https://doi.org/10.1007/s11071-021-06617-7.

22. S. Pal, A. Chatterjee, Dynamics of the interaction of plankton and planktivorous fish with delay, *Cogent Math.*, **2**(1):1074337, 2015, https://doi.org/10.1080/23311835.2015.1074337.

23. M. Rehim, M. Imran, Dynamical analysis of a delay model of phytoplankton–zooplankton interaction, *Appl. Math. Modelling*, **36**(2):638–647, 2012, https://doi.org/10.1016/j.apm.2011.07.018.

24. A. Sharma, A.K. Sharma, K. Agnihotri, The dynamic of plankton–nutrient interaction with delay, *Appl. Math. Comput.*, **231**:503–515, 2014, https://doi.org/10.1016/j.amc.2014.01.042.

25. R. Singh, S. K. Tiwari, A. Ojha, N.K. Thakur, Dynamical study of nutrient-phytoplankton model with toxicity: Effect of diffusion and time delay, *Math. Methods Appl. Sci.*, **46**(1):490–509, 2023, https://doi.org/10.1002/mma.8523.

26. H.L. Smith, *An Introduction to Delay Differential Equations with Applications to the Life Sciences*, Volume 57, Springer, New York, 2011.

27. N.K. Thakur, A. Ojha, Complex plankton dynamics induced by adaptation and defense, *Model. Earth Syst. Environ.*, **6**:907–916, 2020, https://doi.org/10.1007/s40808-020-00727-8.

28. N.K. Thakur, A. Ojha, D. Jana, R.K. Upadhyay, Modeling the plankton–fish dynamics with top predator interference and multiple gestation delays, *Nonlinear Dyn.*, **100**:4003–4029, 2020, https://doi.org/10.1007/s11071-020-05688-2.

29. N.K. Thakur, A. Ojha, P.K. Tiwari, R.K. Upadhyay, An investigation of delay induced stability transition in nutrient-plankton systems, *Chaos Solitons Fractals*, **142**:110474, 2021, https://doi.org/10.1016/j.chaos.2020.110474.

30. N.K. Thakur, R. Singh, A. Ojha, Dynamical study of harmful algal bloom in Sundarban mangrove wetland with spatial interaction and competing effects, *Model. Earth Syst. Environ.*, pp. 1–23, 2022, https://doi.org/10.1007/s40808-021-01088-6.

31. N.K. Thakur, S.K. Tiwari, B. Dubey, R.K. Upadhyay, Diffusive three species plankton model in the presence of toxic prey: Application to Sundarban mangrove wetland, *J. Biol. Syst.*, **25**(02):185–206, 2017, https://doi.org/10.1142/S0218339017500103.

32. R.K. Upadhyay, S. Kumari, P. Kumar, V. Rai, Spatial distribution of microalgae in marine systems: A reaction–diffusion model, *Ecol. Complexity*, **39**:100771, 2019, https://doi.org/10.1016/j.ecocom.2019.100771.

33. Y. Wang, H. Wang, W. Jiang, Stability switches and global Hopf bifurcation in a nutrient-plankton model, *Nonlinear Dyn.*, **78**:981–994, 2014, https://doi.org/10.1007/s11071-014-1491-1.

34. Y. Xiao, L. Chen, Modeling and analysis of a predator–prey model with disease in the prey, *Math. Biosci.*, **171**(1):59–82, 2001, https://doi.org/10.1016/S0025-5564(01)00049-9.

35. T. Zhang, W. Wangi, Hopf bifurcation and bistability of a nutrient–phytoplankton–zooplankton model, *Appl. Math. Modelling*, **36**(12):6225–6235, 2012, https://doi.org/10.1016/j.apm.2012.02.012.